2017 IEEE International Conference on Robotics and Automation (ICRA)
Singapore, May 29 - June 3, 2017

Modeling and Analysis of a Laparoscopic Camera's Interaction with Abdomen Tissue

Reza Yazdanpanah A.[1] and Xiaolong Liu[1] and Jindong Tan[1]

Abstract— **Robotic camera systems have recently drawn attention in minimally invasive surgeries(MIS). Control and manipulation of these systems during traversing abdominal cavity is associated with camera-tissue interaction. This paper demonstrates a theoretical and experimental analysis of a wireless laparoscopic camera's interaction with abdominal wall during MIS. A mechanical model is developed to represent the behavior of abdominal wall bulk tissue by considering skin, fat, muscle and connective tissues layers which predicts behavior of the tissue during interaction with laparoscopic camera. The model was implemented in ABAQUS to analyze the camera-tissue interaction and find interaction forces generated during contact and motion with different linear and rotational speeds. Simulations were validated by experiments on porcine tissue which can be used for proper control of insertable camera. A noninvasive method is proposed to measure the mechanical properties of each patient's abdominal wall tissue at start of MIS in order to tune the control system to optimize the interaction depth and opposite forces. This method features preventing overload damage and camera fall during MIS.**

I. INTRODUCTION

Single incision laparoscopic surgery (SILS) and natural orifice translumenal endoscopic surgery (NOTES) are MIS methods which recently have drawn attention, since they can reduce the surgical incisions to minimum and recovery difficulties at post-operative stage [1]. An important challenge in MIS is shared use of incision for surgical instruments and camera trocar which decreases dexterity and video feedback quality.

Several robotic systems have been developed to improve the dexterity of camera systems in surgeries. Hu et al designed laparoscopic camera with DC servo motors for pan and tilt motion and used suturing for fixation [2], [3]. Castro et al designed a wireless laparoscopic camera that uses piercing needle for anchoring [4]. Using suture and pierce mainly will disable the camera system to be translated to a new position inside the abdomen. Wheeled surgical camera systems have been proposed to enable the translation of camera robots to desired locations [5], [6]. The drawback of wheeled systems is the poor and near-horizontal view angle during the surgery which decreases the quality of hand-eye coordination for the surgeon. One possible improvement for these designs is the application of a magnetic driven systems which traverse abdominal wall ceiling and can provide proper view angle for video capturing [7]–[10].

[1] Reza Yazdanpanah Abdolmalaki, Xiaolong Liu and Jindong Tan are with Department of MABE, University of Tennessee, Knoxville, TN 37996, USA ryazdanp@vols.utk.edu, xliu57@utk.edu, tan@utk.edu.

A major drawback of most reviewed studies is ignoring the interaction of surgical robot and soft tissues. Due to complex characteristics of human tissues and its unique behavior under manipulations such as indentation, rotation and translation. An interaction study is crucial to predict the motion of camera robots inside the abdominal cavity for motion control and manipulation [11]. Another disadvantage of current systems is that most of them concentrate on homogeneous tissues like liver. while magnetic driven systems, traverse abdomen tissue which shows different properties based on patients physical condition and surgical area.

A. Problem Description of Insertable Camera

A novel insertable magnetic driven robotic capsule camera system for SILS was designed by Liu et al [12]. External stator controls anchoring, translation and rotation of an insertable robotic capsule camera (Rotor) by adjustment of magnetic field as conceptually shown in Fig. 1(a),(b).

Patient's abdominal wall thickness differs and has its specific properties based on the fat thickness, muscle density, skin features and other physiological parameters. Since the system works based on magnetic field, the distance of stator to rotor is an important factor in controlling the camera capsule. Over-increasing this distance will diminish the anchoring force over the camera capsule and may cause the camera to fall inside the abdominal cavity. Another critical issue in magnetically driven surgery robots is the damage prevention which may arise from intense compressive force between stator and rotor during traversing tissue.

These issues persuades to design a system capable of measuring each patients tissue properties online and in a non-invasive way. This data will be used to estimate the contact forces/torques and finally tune the stator's control system.

The contributions of this paper are: 1) a biomechanical model of bulk abdominal wall tissue is developed to simulate the abdominal wall behavior; 2) finite Element Simulation of wireless insertable capsule camera's interaction with abdominal wall during motion is presented and interaction forces and torques are validated with experiments on excised porcine abdominal wall tissue for different motion speeds, normal loads and abdomen thicknesses; 3) development of a control system for damage prevention and fall prevention during MIS; 4) propose a method for noninvasive, online measurement of biomechanical properties of abdomen tissue during surgery based on the developed model.

978-1-5090-4633-1/17/$31.00 ©2017 IEEE

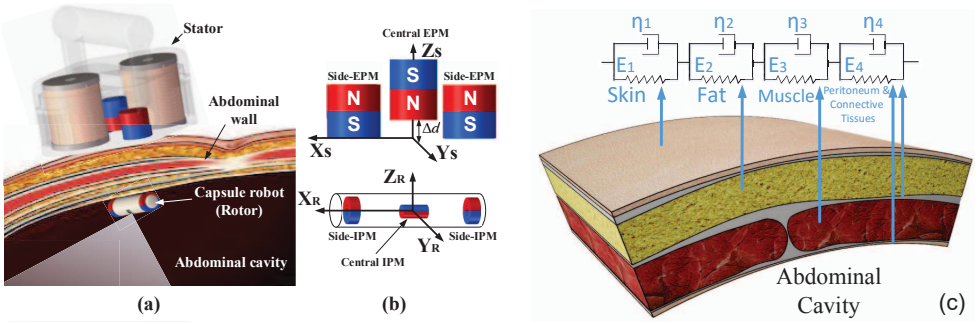

Fig. 1. Wireless insertable capsule camera system. (a) Conceptual illustration of the wireless capsule robot. A stator is placed outside of an insufflated abdominal wall. The capsule robot is anchored, navigated and oriented by the stator to visualize the target surgical area. (b) Configuration of magnets in stator and camera rotor. (c) Mechanical modeling of abdominal tissue with four voigt models in series.

II. MECHANICAL MODELING OF ABDOMINAL WALL TISSUE

A mechanical model is developed to study the bulk abdomen tissue which considers all the major layers of the tissue. Considering the model to do online properties measurement, this model should be simple enough to decrease the simulation complexity, however accurate enough to represent the tissue behavior properly. The accuracy of this model is evaluated by experiment on porcine abdomen tissue specimen.

A. Abdomen Bulk Tissue Model

Living tissues' mechanical behavior is considered as viscoelastic, highly nonlinear, inhomogeneous and anisotropic materials.

A mechanical, viscoelastic model of soft tissues is used to simulate the creep behavior [13]. In this study, since the camera-Tissue interaction during motion in surgery happens in short time ranges, four voigt models in series are used. The proposed model, shown in Fig. 1(c), can simulate the creep behavior of abdominal wall tissue. These four voigt models, each demonstrates a main part of the tissue which are skin, fat, muscle and the connective tissues. Effects of blood vessels and minor layers are also considered in connective tissue model [14].

In this mechanical model, when a constant load σ_0 is applied, the initial displacement will be caused by the springs with moduli E_1, E_2, E_3, E_4 shown in Eq. (1). Compression of dashpots with viscosities of η_1, η_2, η_3 and η_4 will result in following gradual displacements. Summation of these two displacements results in total displacement of tissue under uniaxial load. The total displacement ε of the model can be shown as

$$\varepsilon(t) = \frac{\sigma_0}{E_1}(1 - e^{(\frac{-E_1 t}{\eta_1})}) + \frac{\sigma_0}{E_2}(1 - e^{(\frac{-E_2 t}{\eta_2})}) + \frac{\sigma_0}{E_3}(1 - e^{(\frac{-E_3 t}{\eta_3})}) + \frac{\sigma_0}{E_4}(1 - e^{(\frac{-E_4 t}{\eta_4})}) \quad (1)$$

Parameters of this model can be estimated by creep experiment and measurement of the abdominal wall tissue specimen's displacement versus time.

B. Creep Test

Five specimens of porcine abdominal wall with cross section of $20mm * 20mm$ were cut and were used for creep test. Normal forces of $0.5N$ to $6\ N$ were exerted over the specimens (I) by balance setup introduced in section V and their axial displacement were measured.

Vertical displacements were measured with dial indicator and the measurements were recorded by a 150 fps camera(XIMEA xiQ). The normal load represents the compressive contact force between the camera robot and tissue during surgery. This contact force varies by the camera-stator distance which depends on the patient's abdominal wall thickness. Creep test load's range was selected between $0.5N$ and $6N$ to cover the probable safe contact forces' range

TABLE I

CREEP CRVE FITTED PARAMETERS USED IN THE SIMULATION OF CREEP BEHAVIOR IN PORCINE SPECIMEN

Load (N)	Stiffness (kNm^{-1})				Dashpot viscosity (s)			
σ_0	E_1	E_2	E_3	E_4	η_1	η_2	η_3	η_4
0.5	15.5541	14.6631	14.0707	40.3930	0.6054	1.3378	1.1773	107.0078
1	13.1737	5.8432	5.7823	9.9118	0.4058	0.4828	0.4779	99.9246
2	13.0266	3.8522	3.8664	9.8459	0.3479	0.3296	0.3308	99.8941
3	12.7450	3.3139	3.2974	9.8135	0.3322	0.2834	0.2821	99.8837
4	12.7865	2.9956	2.9798	9.8182	0.2969	0.2560	0.2547	99.8876
5	8.0462	2.5984	3.6073	9.8619	0.3518	0.1083	0.7728	99.7520
6	7.4735	2.7467	3.2855	9.8649	0.3349	0.1135	0.5987	99.9762

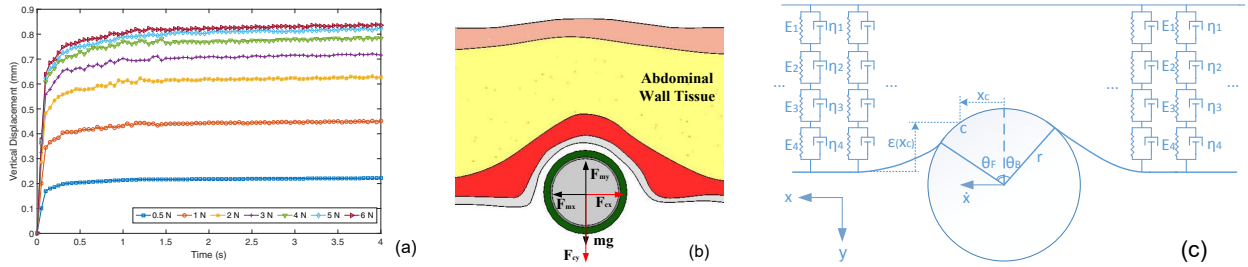

Fig. 2. (a) Results of uniaxial creep test on porcine abdominal wall specimen. (b) Free body diagram of the camera capsule in contact with abdomen (c) Schematic view of camera-tissue contact with 4 Voigt models.

during surgery [15]. Each test was repeated 5 times and the average creep results are shown in Fig. 2(a). An iterative algorithm was used on this raw data to fit the parameters of Equation(1). The proposed four element voigt model parameters, E_1, E_2, E_3, E_4 η_1, η_2, η_3 and η_4 are summarized in Table I for each experiment.

III. Camera-Tissue Interaction Mathematical Model

A mathematical model of Capsule camera-tissue contact is studied which can be used for online estimation of interaction depth in control system. A mathematical model for interaction of wheeled mobile robot and liver tissue was proposed in [16]. The same procedure has been applied here, but the abdominal wall tissue is considered as a generalized kelvin-voigt model for rotation-less translation of camera capsule.

The free body diagram of the camera capsule during interaction with tissue is shown in Fig. 2(b), where F_w shows the gravity force over the capsule. The contact force is shown by F_c which is resolved on x and y axes as F_{cx} and F_{cy} respectively. The magnetic force exerted over the camera is represented as F_m and its components are shown as F_{mx} and F_{my}.

The contact force is generated from different sources during interaction. A simple model has been considered which consists of viscous force of peritoneum fluid which covers the organ and stress from viscoelastic nature of the organ. Due to the small effect of tissue membrane tension it was not considered in this model and the contact force is described as $\mathbf{F}_c = \mathbf{F}_{viscous} + \mathbf{F}_{stress}$.

The stress originated from the displacement of tissue, Due to asymmetry of front and back contact lengths, the resultant stress would be non-zero.

Displacement profile of the membrane in front of the rolling wheel is approximated as a decaying exponential function in the x-direction and also for rolling motion, in the viscoelastic model, the length of contact behind the rolling cylinder is less than front of it due to the viscoelastic nature of the tissue. These assumptions are used for the linear motion modeling and the schematic view of contact is shown in Fig. 2 (c) and the displacement profile is assumed as: $\varepsilon_{(x_c)} = Ae^{B(x_c - C)}$

Where the constant C is the length of contact along x-direction, $C = rsin(\theta_F)$ and r is the radius of capsule camera.

By considering the front contact point at $x_c = rsin(\theta_F)$ and the capsule geometry, the constant A, B are found. The same procedure can be solved for the backside contact point and the displacement profiles can be proposed as

$$\varepsilon(x_c) = \begin{cases} rcos(\theta_F - Y_{center})e^{-\frac{\tan(\theta_F)}{rcos(\theta_F - Y_{center})}(X_c - rsin(\theta_F))} & F \\ rcos(\theta_B - Y_{center})e^{-\frac{\tan(\theta_B)}{rcos(\theta_B - Y_{center})}(X_c - rsin(\theta_B))} & B \end{cases} \tag{2}$$

where F and B stands for Front and Back respectively and Y_{center} is the position of capsule's center of mass on Y-direction.

Finding equations of motions requires to consider the forces acting on the camera capsule along each axis, which are the shear force and the tissue pressure. The shear force generated from the viscous peritoneal fluid covered the internal organs. Due to asymmetry of contact lengths in front and backside, the shear stress generates force on both x and y directions. by projecting the shear force along these axis the generated force can be estimated.

$$F_{Viscous} = \begin{cases} L\int_{\theta_B}^{\theta_A} \tau cos(\theta) r d\theta & x - direxion \\ L\int_{\theta_B}^{\theta_A} \tau sin(\theta) r d\theta & y - direction \end{cases} \tag{3}$$

Where L is the length of camera capsule and τ is shear stress which can be modeled as a newtonian fluid with linear velocity profile in contact region: $\tau = \mu\frac{-\dot{x}cos(\theta)}{h}$

where μ is the peritoneal fluid viscosity and $\dot{x}cos(\theta)$ is the relative linear velocity between camera capsule and the tissue and h is normal distance between these two. μ and h can be calculated experimentally.

The pressure force can be estimated from the displacement of the tissue in contact with capsule camera as follows

$$F_{Stress} = \begin{cases} -L\int_{\theta_B}^{\theta_A} r\sigma(\theta)\tan\theta d\theta & x - direxion \\ L\int_{C_B}^{C_A} \sigma(x_c) dx_c & y - direction \end{cases} \tag{4}$$

where $C_B = r\theta_B$ and $C_F = r\theta_F$ are the back and front contact lengths respectively. Also $\sigma(x_c)$ can be found from the viscoelastic response of the tissue: $\sigma(x_c) = \frac{\varepsilon(x_c)}{\sum_{i=1}^{4}\frac{1}{E_i}(1 - e^{-\frac{E_i}{\eta_i}t})}$

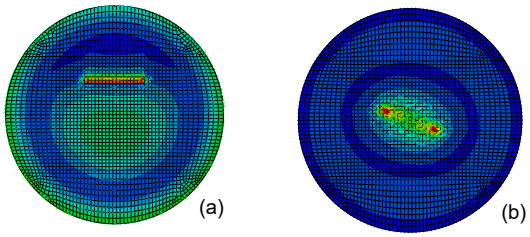

Fig. 3. Finite element simulations of interactions: (a) Contact of camera capsule and tissue during a linear motion with speed of $v = 5\ cm/s$ at time t= 1.6 s. (b) Contact of camera capsule and tissue during a pan motion at time $t = 1\ s$ with the angular velocity of $\omega = \pi/4\ rad/s$.

Considering m as mass of capsule camera, the equations of motion can be formulated as:

$$\begin{cases} m\ddot{x} = F_{mx} + F_{viscous-x} + F_{Tissue_x} & x - direxion \\ m\ddot{y} = mg + F_{viscous-y} + F_{Tissue_y} - F_{my} & y - direction \end{cases} \quad (5)$$

IV. INTERACTION'S FINITE ELEMENT SIMULATION

Interaction of camera capsule and abdomen tissue was simulated in ABAQUS 6.14 to study the contact forces and deformations of the tissue during linear motion and pan motion. Based on the proposed model, properties of each layer was implemented into ABAQUS to replicate porcine tissue. The comparison of creep experiment and simulation reveals less than 5% deviation.

A. Camera-Tissue Interaction

The capsule camera with the length of 80 mm and weight of 50 g is modeled in ABAQUS as an analytical rigid body with 1600 elements. For simulating the abdominal wall tissue, a cylindrical viscoelastic model with radius of 150mm, thickness of 30mm and 30000 elements was considered. Fixed boundary conditions are considered to replicate the experiment. Different Normal forces were exerted over capsule to represent the magnetic force in real experiment which compress the capsule toward abdominal wall. Friction coefficients were considered as 0.1 for static and 0.075 for dynamic.

Two groups of simulation were implemented to test the linear and pan motion separately. Simulation were carried out in two steps, first the gravity and normal concentrated forces are exerted over the capsule. Time $t = 0$ shows the indentation only without any motion. Second step will simulate the motion of capsule camera during contact. Fig.3(a) shows the stresses generated over the tissue during linear motion with constant speed of 10 mm/s. Fig.3(b) shows the contact stresses after 1.776 s during a pan motion with constant angular speed of $\pi/4\ rad/s$.

Contact forces during these motions are exported from ABAQUS. The horizontal force exerted over the camera capsule model during a linear speed motion with different linear speeds is shown in Fig.4(a). After the first second, when the contact is established, the rotor starts to move in horizontal plane with different speeds. Increasing the linear speed results in reduction of contact force. This effect can be justified by the fact that increasing the speed, will reduce the contact depth and will result in less contact force.

The same simulations were run for different speeds of pan motions in order to find the generated torque during constant speed pan motion of camera robot. Angular velocities were chosen in the range of $\omega = \pi/6$ to $\omega = \pi\ rad/s$ to cover the probable actuated pan motion of ex-vivo stator.

B. Different Normal Forces versus Contact Forces

Based on the thickness of patient's abdominal wall, distance of stator to rotor would change and consequently, the normal attractive force between magnets will vary. Different normal interaction forces of the camera capsule and the contact were simulated for a case of linear speed $v = 5\ cm/s$. Generated horizontal force shows that by increasing the normal contact force, the generated lateral force would increase which is a rational result. Since increasing the normal force would increase the friction force between rigid capsule and soft tissue, also the depth of indentation would increase which leads to more resistant force.

V. EXPERIMENTS

In this section, design of experiments will be discussed. All the experiments are done on the basis of the balance setup. This balance setup has sub-gram resolution in weight measuring, 0.0254mm resolution in displacement measurements and has the feature to cancel the indicator spring force for the experiments while keeping a constant-load contact during the motion of tissue below the camera capsule.

A. Tissue Specimen

For the experiment excised porcine abdominal wall was used. $20mm * 20mm$ cross section specimens were cut for creep test. Each specimen contains different layers of skin, fat, muscle and connective tissues. A $150mm * 150mm$ cross section of abdominal wall was used for measuring the contact forces during linear motion and pan motion of capsule camera over the tissue.

B. Experimental Setup

A balance setup was designed to run the experiment with high accuracy in measuring the normal displacement and the normal force exerted over the tissue. For this purpose two identical dial indicators(All Industrial Inc.) with the resolution of 0.0254mm were used on the two opposite sides of the balance setup as shown in Fig.5(a). since the range of Displacement is less than 3mm, by pre-adjusting both indicators to 10mm, it can be assumed that the springs are linear and cancel each other during measurements. This design also helps to keep the contact during the whole motion and overcome the oscillations.

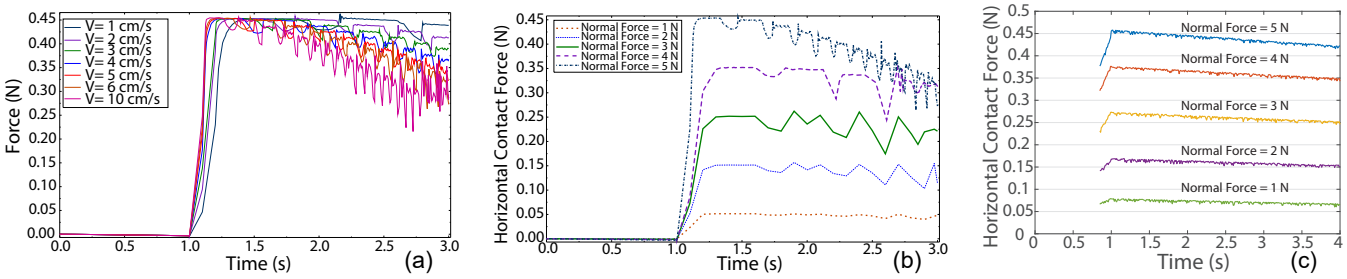

Fig. 4. FEM simulations and experiments of linear motion interactions: (a) Horizontal contact force generated during linear motion of camera with different linear speeds in ABAQUS with normal force of $5N$. The first second, is the indentation step and the horizontal contact force is zero. (b) Different normal forces were exerted over capsule camera and generated horizontal contact force were simulated during a linear motion of $v = 5\ cm/s$. (c) Experiment result for measuring generated horizontal force with a linear motion of $v = 5\ cm/s$ under different normal forces. The first 1 second is considered for proper indentation of camera capsule over the tissue and measurements are started at $t = 0.85s$.

C. Linear and Pan Motion Interaction Force Detection

Purpose of this experiment is to find the required horizontal force which should be exerted on camera capsule to move with constant linear speed during interaction with soft tissue. This force can be used to estimate the force generated by interaction during traversing of abdominal wall. For this experiment the balance setup was used and a constant mass of 200 g were used to exert normal force over the camera capsule over the tissue while camera capsule was fixed to the balance setup. The tissue below the camera was driven by a servo motor at constant speed of 1 cm/s and the horizontal force created by interaction was measured by a six axis force/torque(F/T) sensor (HEX-58-RB-2000N, OptoForce Inc.) as shown in Fig.5(b).

The same procedure as linear motion experiment was used for pan motion experiment as shown in Fig.5(c). Different angular velocities with the range of $\omega = \pi/6$ to $\omega = \pi\ rad/s$ were tested to measure the torque generated during contact. A comparison of simulation and experiment reveals good compliance.

D. Interaction Force Test

A set of experiments were done to find the effect of normal force on generated contact force during a constant speed linear motion. The normal force range was selected as 1 N to 5 N with a constant speed of $v = 5\ cm/s$. The results of this experiment are shown in Fig.4(c) and comparison with the ABAQUS simulation analysis results shows a good compliance.

VI. DAMAGE PREVENTION, FALL PREVENTION AND ONLINE TISSUE PROPERTIES MEASUREMENT SYSTEM

Due to the lack of haptic feedback in robot-assisted MIS, tool-tissue overload may result in collateral tissue damage. in order to minimize tissue damage in MIS, a force control strategy seems crucial. By knowing damage thresholds for abdomen tissue, it can be incorporated into the control scheme so that instrument forces are limited to this level and tissue overload is actively prevented and prevent actuator failures [15], [17].

A stator-rotor distance estimation mechanism was designed in our previous work [10]. Different parameters of this mechanism are defined in Fig.6(a). D is the distance between stator and patient's stomach and can be adjusted by an arm robot, controlling the stator's position and orientation. By attaching two miniature force sensors (Tekscan FlexiForce A101) to the external shell of camera capsule, we can measure the contact force (F_{-c}) online during the tissue interaction (Fig.6(b). System initially measures the distance of stator to rotor (h) and the sensed contact force will be compared to the desired contact force. Deviation from desired force will cause the stator-holder arm robot to adjust the stator-rotor distance (D).

The benefits of contact force control system are: 1) it reduces possibility of collateral injuries caused by force overload during surgery; 2) an important aspect in magnetic driven camera systems is fall preventing assurancecaused by loss of anchoring force. This control system can prevent the falling by limiting the stator-rotor distance based on sensed force and always keep (h) in the range where $F_{min} < F_{-c} <$

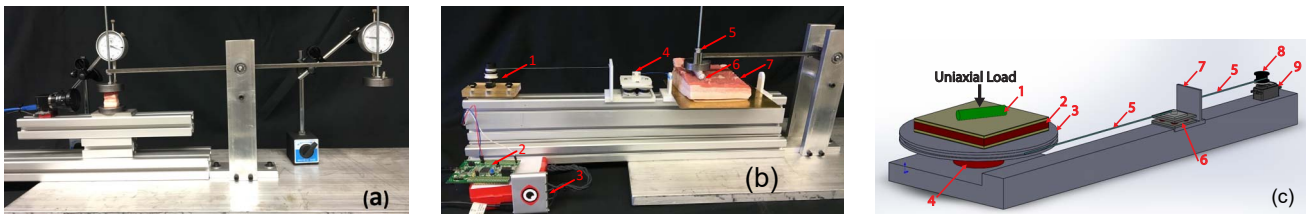

Fig. 5. (a)Balance setup. (b) Linear motion experiment to measure lateral interaction force: 1-Servo motor 2-STM32 microController 3-OptoForce force sensor 4-Force sensor DAQ 5-Normalload weights 6-Camera capsule 7-Porcine abdominal wall tissue. (c) Pan experiment setup consists of : 1- Camera robot. 2- Abdominal wall tissue. 3- Rotating disk. 4- Bearing. 5- Strings. 6- Force sensor. 7- Sliding base of Force sensor. 8- Pulley. 9- Servo Motor.

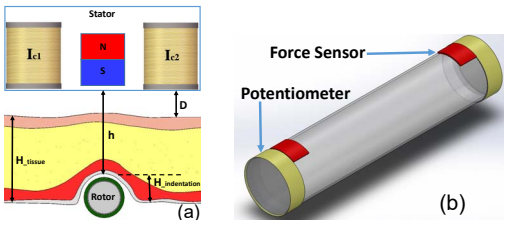

Fig. 6. (a) Force estimation system. h is stator-Rotor distance estimated by hall effective sensors. D is distance of stator and patient's stomach. H_tissue is abdomen's thickness. $H_{-indentation}$ is camera's indentation depth caused by magnetic pull. (b) Camera capsule with force sensor to sense contact normal force and potentiometer to sense indentation depth.

F_{max}.

A. Online Tissue Properties Measurement

Patient's physical condition and obesity influence magnetic driven system's performance and control. Abdominal wall thickness features has influence on the properties of tissue. These properties are different for each patient and even different for abdomen areas, As a result the camera-tissue interaction depth and forces will be variable. In order to control the camera inside the abdominal cavity, interaction forces should be estimated online and used to the control system. Finding the interaction forces requires an online tissue properties measurement system.

A method has been developed here in order to measure properties of tissue online. The main idea is to regenerate the creep test in-vivo with camera and stator. The system measures indentation depth $H_{-indentation}$ during interaction by Two ribbon potentiometers attached over the camera capsule. The resistance measured by potentiometers demonstrates the length of contact. As shown in Fig.2(c) the length of contact can be shown as $r(\theta_F + \theta_B)$. The online creep test is done in static state so $\theta_F = \theta_B$. By using the exponential profile defined in section III, The real indentation depth can be measured. Online properties measurement is done at beginning of camera insertion and indentation data versus time gives creep response of specific patient's tissue. The creep test data will be implemented in the mechanical model of section II to generate contact forces and control system will be tuned.

VII. CONCLUSION AND FUTURE WORK

In this paper, interaction of a wireless insertable laparoscopy camera and abdominal wall tissue during motion is studied. First an accurate mechanical model of abdominal wall tissue was derived to represent the complex behavior of alive tissues during interaction. The creep experiment helped to find the parameters of the model and finite element analysis confirmed the model. The camera system we studied, features pan and linear motion, so these motions were simulated in ABAQUS to find the interaction forces. Comparisons show good compliance between simulation and experiment results. These results were validated by linear and pan motion interaction experiments designed over a bulk porcine abdominal wall.

An online noninvasive property measurement system is proposed which can use this model. This system will provide the required data for stator's control system for each specific patient during surgery. It also prevents the force overload of tissue and can cancel camera fall during the MIS. In our future work, a closed loop control system will be developed to control camera motion during interaction based on the normal and horizontal contact forces. The insertable wireless camera system will be used for laparoscopy surgery on alive pigs.

REFERENCES

[1] P. Valdastri, M. Simi, and R. J. Webster III, "Advanced technologies for gastrointestinal endoscopy," *Annual review of biomedical engineering*, vol. 14, pp. 397–429, 2012.

[2] J. Westwood *et al.*, "In-vivo stereoscopic imaging system with 5 degrees-of-freedom for minimal access surgery," *Medicine Meets Virtual Reality 12: Building a Better You: the Next Tools for Medical Education, Diagnosis, and Care*, vol. 98, p. 234, 2004.

[3] T. Hu, P. K. Allen, and D. L. Fowler, "In-vivo pan/tilt endoscope with integrated light source," in *Intelligent Robots and Systems, 2007. IROS 2007. IEEE/RSJ International Conference on*, pp. 1284–1289, IEEE, 2007.

[4] C. A. Castro, A. Alqassis, S. Smith, T. Ketterl, Y. Sun, S. Ross, A. Rosemurgy, P. P. Savage, and R. D. Gitlin, "A wireless robot for networked laparoscopy," *Biomedical Engineering, IEEE Transactions on*, vol. 60, no. 4, pp. 930–936, 2013.

[5] M. E. Rentschler, J. Dumpert, S. R. Platt, K. Iagnemma, D. Oleynikov, and S. M. Farritor, "An in vivo mobile robot for surgical vision and task assistance," *Journal of Medical Devices*, vol. 1, no. 1, pp. 23–29, 2007.

[6] M. E. Rentschler, J. Dumpert, S. R. Platt, K. Lagnemma, D. Oleynikov, and S. M. Farritor, "Modeling, analysis, and experimental study of in vivo wheeled robotic mobility," *IEEE Transactions on Robotics*, vol. 22, no. 2, pp. 308–321, 2006.

[7] F. Leong, N. Garbin, C. Di Natali, A. Mohammadi, D. Thiruchelvam, D. Oetomo, and P. Valdastri, "Magnetic surgical instruments for robotic abdominal surgery," *IEEE reviews in biomedical engineering*, vol. 9, pp. 66–78, 2016.

[8] M. Salerno, S. Tognarelli, C. Quaglia, P. Dario, and A. Menciassi, "Anchoring frame for intra-abdominal surgery," *The International Journal of Robotics Research*, vol. 32, no. 3, pp. 360–370, 2013.

[9] S. Tognarelli, M. Salerno, G. Tortora, C. Quaglia, P. Dario, and A. Menciassi, "An endoluminal robotic platform for minimally invasive surgery," in *Biomedical Robotics and Biomechatronics (BioRob), 2012 4th IEEE RAS & EMBS International Conference on*, pp. 7–12, IEEE, 2012.

[10] X. Liu, A. R. Yazdanpanah, G. J. Mancini, and J. Tan, "Control of a magnetic actuated robotic surgical camera system for single incision laparoscopic surgery," in *Robotics and Biomimetics (ROBIO), 2015 IEEE International Conference on*, pp. 1396–1402, IEEE, 2015.

[11] Y.-C. Fung, *Biomechanics: mechanical properties of living tissues*. Springer Science & Business Media, 2013.

[12] X. Liu, G. J. Mancini, Y. Guan, and J. Tan, "Design of a magnetic actuated fully insertable robotic camera system for single-incision laparoscopic surgery," *IEEE/ASME Transactions on Mechatronics*, vol. 21, no. 4, pp. 1966–1976, 2016.

[13] S. Arıtan, S. O. Oyadiji, and R. M. Bartlett, "A mechanical model representation of the in vivo creep behaviour of muscular bulk tissue," *Journal of biomechanics*, vol. 41, no. 12, pp. 2760–2765, 2008.

[14] S. Standring, *Gray's anatomy: the anatomical basis of clinical practice*. Elsevier Health Sciences, 2015.

[15] N. Famaey, E. Verbeken, S. Vinckier, B. Willaert, P. Herijgers, and J. Vander Sloten, "In vivo soft tissue damage assessment for applications in surgery," *Medical engineering & physics*, vol. 32, no. 5, pp. 437–443, 2010.

[16] M. E. Rentschler, *In vivo abdominal surgical robotics: Tissue mechanics modeling, robotic design, experimentation, and analysis*. PhD thesis, Univ. of Nebraska-Lincoln, 2006.

[17] M. E. Raoufat, K. Tomsovic, and S. M. Djouadi, "Virtual actuators for wide-area damping control of power systems," *IEEE Transactions on Power Systems*, vol. 31, no. 6, pp. 4703–4711, 2016.